Linear and nonlinear particle-magnetohydrodynamic simulations of the toroidal Alfven eigenmode

Linear and nonlinear particle-magnetohydrodynamic simulations of the toroidal Alfvén eigenmode

Y. Todo[a] and T. Sato
Theory and Computer Simulation Center, National Institute for Fusion Science, 322-6 Oroshi-cho, Toki, Gifu 509-5292, Japan

(Received 2 January 1998; accepted 14 January 1998)

Linear and nonlinear particle-magnetohydrodynamic (MHD) simulation codes are developed to study interactions between energetic ions and MHD modes. Energetic alpha particles with the slowing-down distribution are considered and the behavior of $n=2$ toroidal Alfvén eigenmodes (TAE modes) is investigated with the parameters pertinent to the present large tokamaks. The linear simulation reveals the resonance condition between alpha particles and TAE mode. In the nonlinear simulation, two $n=2$ TAE modes are destabilized and alpha particle losses induced thereby are observed. Counterpassing particles are lost when they cross the passing-trapped boundary. They are the major part of lost particles, but trapped particles are also lost appreciably. © *1998 American Institute of Physics.* [S1070-664X(98)02405-7]

I. INTRODUCTION

Successful confinement of energetic alpha particles is required for self-sustained operation of fusion reactors. The alpha particles born from deuterium–tritium (D–T) reactions are supposed to destabilize the toroidal Alfvén eigenmode (TAE mode).[1] Nonlinear behaviors of the TAE mode and alpha particles are one of the major uncertainties for fusion reactor physics. The mechanism of alpha-particle losses induced by a single TAE mode was investigated by a Monte Carlo simulation in Ref. 2. They found that crossing the passing-trapped boundary is a dominant process of the alpha-particle loss induced by a single mode. They also found that the fraction of lost particles depends on the amplitude of the TAE mode. Thus, nonlinear evolutions of the TAE mode and alpha particles must be known for designing a fusion reactor.

Recently, theoretical and computational studies[3–6] have shown that wave trapping of resonant particles works as a saturation mechanism of a single TAE mode. It is, however, not clear that the wave–particle trapping works as the dominant saturation mechanism when a large number of TAE modes are destabilized. For larger tokamaks such as the International Thermonuclear Experimental Reactor (ITER) high-n TAE modes are predicted to be most dangerous.[7,8] With a relevant q profile a large number of TAE modes can be destabilized simultaneously. In such cases resonance overlap is predicted to take place[9] and wave–particle trapping will be prevented by the other TAE modes. Therefore, we suppose that magnetohydrodynamic (MHD) nonlinearities such as proposed in Refs. 10 and 11, survive as potential candidates for saturation mechanism.

This gives us a sufficient motivation to develop a simulation code with nonlinear MHD equations. We employ a kinetic–MHD hybrid model[12,5] where plasma is divided into two parts, i.e., alpha particles and background plasma. The particle simulation method is used for the alpha-particle component, while the background plasma is described by the full MHD equations which are solved by a finite difference method. In addition to the nonlinear code, its linear version is also developed. In this paper, we describe the results of linear and nonlinear particle–MHD simulations and demonstrate that the two codes are useful tools to study the alpha–TAE dynamics.

Compared with previous works[4,5] where magnetic moments of alpha particles are set to be zero, the present work has an advantage that a more realistic alpha-particle distribution can be considered. A realistic alpha-particle distribution is really indispensable to the study of alpha-particle losses.

The plasma model and the computational method are described in Sec. II. Section III is devoted to results of linear particle–MHD simulation. The structure of the most unstable TAE mode and the resonance condition are investigated with the linear simulation. The resonance condition is important to understanding alpha-particle losses in the nonlinear simulation. The results of nonlinear particle–MHD simulation are described in Sec. IV. Two cases where the initial alpha-particle pressure is changed are investigated. For the high-alpha-pressure case, another $n=2$ TAE mode is destabilized and alpha-particle losses induced by TAE modes are examined. A summary is given in Sec. V.

II. SIMULATION MODEL AND COMPUTATIONAL METHOD

In the model employed here, plasma is divided into two parts, the background plasma and alpha particles. The background plasma is described by the ideal MHD equations and the electromagnetic field is given by the MHD description. This approximation is reasonable under the condition that the alpha density is much less than the background plasma density. The ideal MHD equations are

$$\frac{\partial \rho}{\partial t} = -\nabla \cdot (\rho \mathbf{v}), \tag{1}$$

[a]Electronic mail: todo@nifs.ac.jp

$$\rho \frac{\partial}{\partial t}\mathbf{v}+\rho\mathbf{v}\cdot\nabla\mathbf{v}=-\nabla p+\frac{1}{\mu_0}(\nabla\times\mathbf{B})\times\mathbf{B}, \tag{2}$$

$$\frac{\partial\mathbf{B}}{\partial t}=-\nabla\times\mathbf{E}, \tag{3}$$

$$\frac{\partial p}{\partial t}=-\nabla\cdot(p\mathbf{v})-(\gamma-1)p\nabla\cdot\mathbf{v}, \tag{4}$$

$$\mathbf{E}=-\mathbf{v}\times\mathbf{B}, \tag{5}$$

where μ_0 is the vacuum magnetic permeability, γ is the adiabatic constant, and all other quantities are conventional.

The drift-kinetic description is employed for the alpha particles. The guiding-center velocity $\mathbf{u}$ is given by

$$\mathbf{u}=\mathbf{v}_\parallel^*+\mathbf{v}_E+\mathbf{v}_B, \tag{6}$$

$$\mathbf{v}_\parallel^*=\frac{v_\parallel}{B}[\mathbf{B}+\rho_\parallel B\nabla\times\mathbf{b}], \tag{7}$$

$$\mathbf{v}_E=\frac{1}{B}[\mathbf{E}\times\mathbf{b}], \tag{8}$$

$$\mathbf{v}_B=\frac{1}{q_\alpha B}[-\mu\nabla\mathbf{B}\times\mathbf{b}], \tag{9}$$

$$\rho_\parallel=\frac{m_\alpha v_\parallel}{q_\alpha B}, \tag{10}$$

$$\mathbf{b}=\mathbf{B}/B, \tag{11}$$

$$m_\alpha v_\parallel\frac{dv_\parallel}{dt}=\mathbf{v}_\parallel^*\cdot[q_\alpha\mathbf{E}-\mu\nabla B], \tag{12}$$

where $v_\parallel$ is the velocity parallel to the magnetic field and μ is the magnetic moment, which is the adiabatic invariant.

To complete the equation system in a self-contained way, we take account of the effects of the alpha particles on the background plasma in the MHD momentum equation. We can now give a more transparent derivation of the model than in Refs. 5 and 12. The background plasma is affected by the electromagnetic field through its charge and current densities which can be calculated from those of the total plasma and the alpha particles. Thus, the momentum equation for the background plasma is

$$\rho \frac{\partial}{\partial t}\mathbf{v}+\rho\mathbf{v}\cdot\nabla\mathbf{v}=(Q-Q_\alpha)\mathbf{E}+\left(\frac{1}{\mu_0}\nabla\times\mathbf{B}-\mathbf{j}_\alpha\right)\times\mathbf{B}-\nabla p, \tag{13}$$

$$\mathbf{j}_\alpha=\int\mathbf{u}fd^3v+\nabla\times\mathbf{M}, \tag{14}$$

$$\mathbf{M}=-\int\mu\mathbf{b}fd^3v, \tag{15}$$

where Q and Q_α are the total charge density and alpha-particle charge density, and $\mathbf{j}_\alpha$ is the alpha-particle current density. The total charge density Q is negligible in the MHD approximation where the quasineutrality is satisfied. Equation (13) can be rewritten into the following form paying attention to the fact that $-Q_\alpha\mathbf{E}$ cancels out with the Lorentz force due to $\mathbf{E}\times\mathbf{B}$ current of alpha particles:

$$\rho \frac{\partial}{\partial t}\mathbf{v}+\rho\mathbf{v}\cdot\nabla\mathbf{v}=\left(\frac{1}{\mu_0}\nabla\times\mathbf{B}-\mathbf{j}'_\alpha\right)\times\mathbf{B}-\nabla p, \tag{16}$$

$$\mathbf{j}'_\alpha\equiv\int(\mathbf{v}_\parallel^*+\mathbf{v}_B)fd^3v+\nabla\times\mathbf{M}$$
$$=\mathbf{j}_{\alpha\parallel}+\frac{1}{B}(P_{\alpha\parallel}\nabla\times\mathbf{b}-P_{\alpha\perp}\nabla\ln B\times\mathbf{b})$$
$$-\nabla\times\left(\frac{P_{\alpha\perp}}{B}\mathbf{b}\right). \tag{17}$$

It is interesting to note that if the alpha-particle distribution is isotropic in the velocity space (i.e., $P_{\alpha\parallel}=P_{\alpha\perp}\equiv P_\alpha$), Eq. (16) has an exact simple form, i.e.,

$$\rho \frac{\partial}{\partial t}\mathbf{v}+\rho\mathbf{v}\cdot\nabla\mathbf{v}=\frac{1}{\mu_0}(\nabla\times\mathbf{B})\times\mathbf{B}-\nabla P_\alpha-\nabla p. \tag{18}$$

Alpha-particle distribution, however, is not isotropic in general. Therefore, we should use Eq. (16) instead of Eq. (18).

We use the δf method[13,14] for the alpha particles. Time evolution of the weight of the jth particle is described by[14]

$$\frac{d}{dt}w_j=-(1-w_j)\left[(\mathbf{v}_E+v_\parallel\delta\mathbf{b})\cdot\nabla+\left(\frac{dv_\parallel}{dt}\right)_1\frac{\partial}{\partial v_\parallel}\right]\ln f_0, \tag{19}$$

$$\left(\frac{dv_\parallel}{dt}\right)_1=[\mathbf{b}+\rho_\parallel\nabla\times\mathbf{b}]\cdot\left[\frac{q}{m}\mathbf{E}\right]+\delta\mathbf{b}\cdot\left[-\frac{\mu}{m}\nabla B\right], \tag{20}$$

$$\delta\mathbf{b}=\mathbf{b}-\mathbf{b}_0, \tag{21}$$

where f_0 is the initial distribution which is a function of the magnetic surface and energy. Using this weight, the alpha-particle current $\mathbf{j}'_\alpha$ in Eq. (17) is evaluated through

$$P_{\alpha\parallel}=P_{\alpha\parallel0}+\sum_j w_j m_\alpha v_{\parallel j}^2 S(\mathbf{x}-\mathbf{X}_j), \tag{22}$$

$$P_{\alpha\perp}=P_{\alpha\perp0}+B\sum_j w_j\mu_j S(\mathbf{x}-\mathbf{X}_j), \tag{23}$$

where $S(\mathbf{x}-\mathbf{X}_j)$ is the shape factor of each super particle.

The initial condition is a MHD equilibrium where the total plasma beta is 4% at the magnetic axis and its volume average is 0.88%. The initial alpha-particle distribution is the slowing-down distribution which is isotropic in the velocity space with the maximum energy of 3.5 MeV. Particles are distributed from 0.1 to 3.5 MeV. The background plasma is supposed to be a D–T plasma with the number density of 10^{20} m^{-3}. The magnetic field strength at the magnetic axis, the minor radius, and the aspect ratio are 5 T, 0.9 m, and 3, respectively. With these parameters, the velocity of an alpha particle whose energy is 1 MeV is equal to the Alfvén velocity. The cylindrical coordinate system (R,φ,z) is used in simulations. The simulation region is $2a\leqslant R\leqslant 4a$, $-a\leqslant z\leqslant a$ where a is the minor radius. The magnetic axis locates at $R=R_0\equiv 3.20a$, $z=0$.

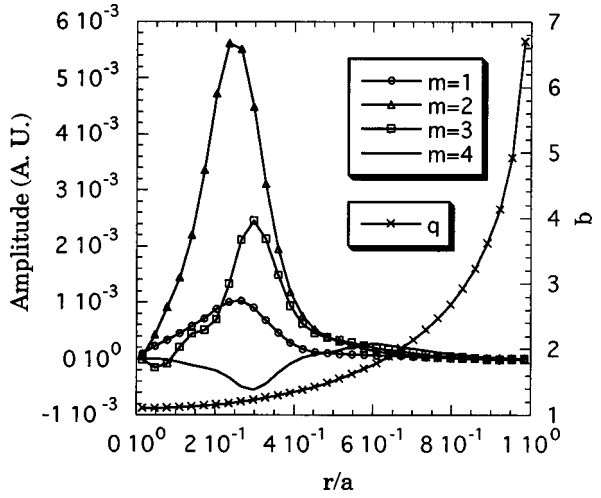

FIG. 1. Radial profiles of the dominant poloidal harmonics of the electrostatic potential for the most unstable $n=2$ TAE mode.

For analysis of simulation data, a flux coordinate system (r,φ,θ) is constructed. In this coordinate system, the equilibrium magnetic field $(B_{0r},B_{0\varphi},B_{0\theta})$ is parallel to $(0,1,-1/q)$, where q is the safety factor. The q profile is shown in Fig. 1 with the poloidal harmonics of the most unstable $n=2$ TAE mode, which is discussed in Sec. III.

III. LINEAR SIMULATION

We have proposed a linear simulation technique[15] where Eqs. (1)–(5) and (19) are linearized. Particles are followed along their equilibrium orbits. An essential difference of this method from the nonlinear δf method is that the superparticles are employed to sample elements of the four-dimensional phase space $(R,z,v_\parallel,\mu)$ instead of the five-dimensional phase space $(R,\varphi,z,v_\parallel,\mu)$. Dependence of the distribution function on the φ direction is evaluated through a particle weight which is a function of φ. Equation (19) is transformed into

$$\frac{D}{Dt}w_j(\varphi)+u_{0\varphi}\frac{\partial}{R\partial\varphi}w_j(\varphi)$$

$$=-\frac{1}{f_0}\left[(\mathbf{v}_E+v_\parallel\delta\mathbf{b})\cdot\nabla f_0+\left(\frac{dv_\parallel}{dt}\right)_1\frac{\partial}{\partial v_\parallel}f_0\right], \tag{24}$$

$$\frac{D}{Dt}\equiv\frac{\partial}{\partial t}+u_{0R}\frac{\partial}{\partial R}+u_{0z}\frac{\partial}{\partial z}+\left(\frac{dv_\parallel}{dt}\right)_0\frac{\partial}{\partial v_\parallel}, \tag{25}$$

where the subscript ''0'' of the velocities and the acceleration denotes that they are evaluated along the equilibrium orbits. We express the weight function and the electromagnetic field with a toroidal Fourier mode n such as

$$w_j(\varphi)=w_j^\dagger e^{in\varphi}. \tag{26}$$

Equation (24) is rewritten as

$$\frac{D}{Dt}w_j^\dagger=-\frac{inu_{0\varphi}}{R}w_j^\dagger-\frac{1}{f_0}\left[(\mathbf{v}_E^\dagger+v_\parallel\delta\mathbf{b}^\dagger)\cdot\nabla f_0+\left(\frac{dv_\parallel}{dt}\right)_1^\dagger\frac{\partial}{\partial v_\parallel}f_0\right]. \tag{27}$$

The linear simulation technique has an advantage against the nonlinear δf technique that it is less demanding in CPU time and memory, since the phase space which must be filled with super particles is reduced from five dimension to four dimension. The number of particles used is 2.6×10^5 in the linear simulation, which is much less than 4.0×10^6 in the nonlinear simulation. We carried out test runs of linear and nonlinear simulations, and confirmed that they give consistent results with each other, in linear growth rate, real frequency, and mode structure. The grid numbers used for the poloidal plane (R,z) are (65,65). The initial volume-average beta of alpha particles $(\langle\beta_\alpha\rangle)$ is 0.44% for the linear simulation.

The linear simulation gives the most unstable mode for each toroidal mode number. For the $n=2$ mode, we find that the $n=2$ TAE mode which consists mainly of $m=2$ and $m=3$ harmonics has the largest growth rate. Figure 1 shows the radial profiles of the dominant poloidal harmonics for the $n=2$ TAE mode. The real frequency ω_0 is $0.36\omega_A$ whose absolute value is lower by $0.04\omega_A$ than the gap center at $q=5/4$. Since we restrict n to be positive, ω_0 can take both positive and negative signs within the framework of MHD. Energetic alpha particles break the symmetry of MHD theory and destabilize a TAE mode which rotates in the same poloidal direction as the diamagnetic drift of alpha particles.

We also investigate the resonance condition of alpha particles with the TAE mode. When a resonant particle passes one round in the poloidal angle, the phase of the TAE mode at the location of the particle should change by a multiple of 2π. Thus, we expect that the resonance condition is given by

$$\omega_0 T_\theta - n\Delta\varphi = 2l\pi, \tag{28}$$

where T_θ, $\Delta\varphi$, and l are the time for each particle to pass one round in the poloidal angle, the toroidal angle which the particle passes in T_θ, and an arbitrary integer, respectively. We divide Eq. (28) by T_θ and obtain

$$\omega_0 - n\omega_\varphi - l\omega_\theta = 0, \tag{29}$$

or

$$l=(\omega_0-n\omega_\varphi)/\omega_\theta, \tag{30}$$

where $\omega_\theta=2\pi/T_\theta$ and $\omega_\varphi=\Delta\varphi/T_\theta$.

We measure ω_θ and ω_φ of all particles, and calculate l of each particle from Eq. (30). Alpha particles are put in the order of energy transfer to the TAE mode in order to classify them into strongly resonant particles, weakly resonant particles, and nonresonant particles. First we pick up the top 2000 particles as strongly resonant particles which cover 67% of the total energy transfer. The values of l are plotted in Fig. 2(a). It can be seen that strongly resonant particles have values of l actually close to integers. Thus, we can conclude that the resonance condition is Eq. (29) or Eq. (30).

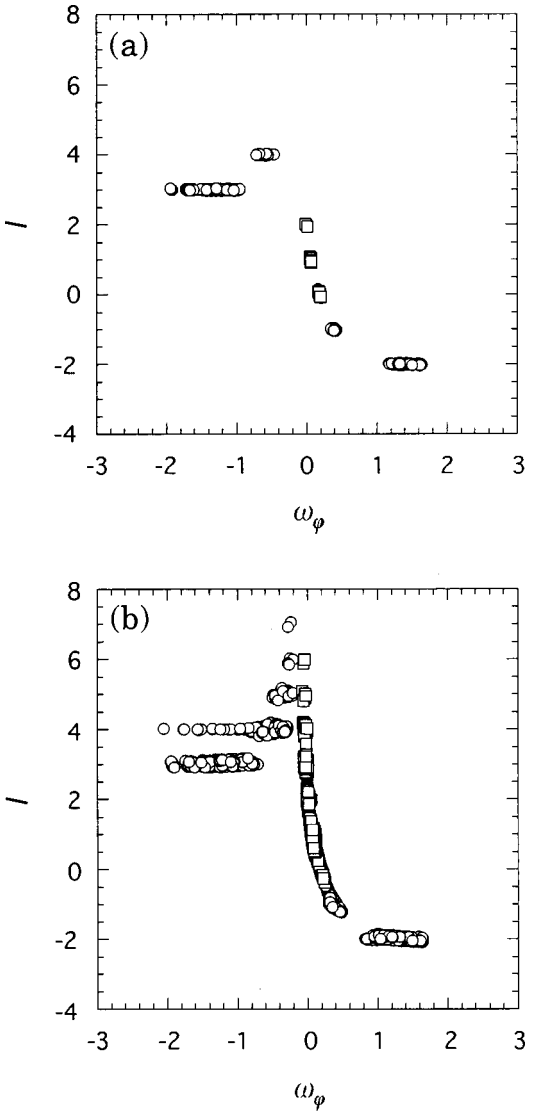

FIG. 2. Resonance condition of alpha particles to the most unstable $n=2$ TAE mode for the (a) top 2000 particles, and (b) top 8000 particles. Circles denote passing particles and squares denote trapped particles.

In Fig. 2(a) we can see that the dominant resonances are $l=3$ for $\omega_\varphi<0$ and $l=-2$ for $\omega_\varphi>0$ for passing particles. We can explain it as follows for a passing particle whose magnetic moment is much smaller than the energy divided by the magnetic field strength (hereafter, we refer to such a particle as a ''far-passing particle''). First, the local parallel phase velocity of the m harmonic of the TAE mode, denoted as V_m, approximately satisfies

$$\omega_0 \simeq V_m k_{\parallel m}, \tag{31}$$

where $k_{\parallel m}=(n-m/q)/R_0$. For far-passing particles resonant with the m harmonic of the TAE mode, ω_φ and ω_θ can approximate V_m/R_0 and $|V_m/(-qR_0)|$, respectively. We substitute Eq. (31) and these approximations into Eq. (29) and obtain

$$V_m(n-m/q)/R_0 - nV_m/R_0 - l|V_m/(-qR_0)| = 0. \tag{32}$$

Finally, we reach the following resonance condition for far-passing particles:

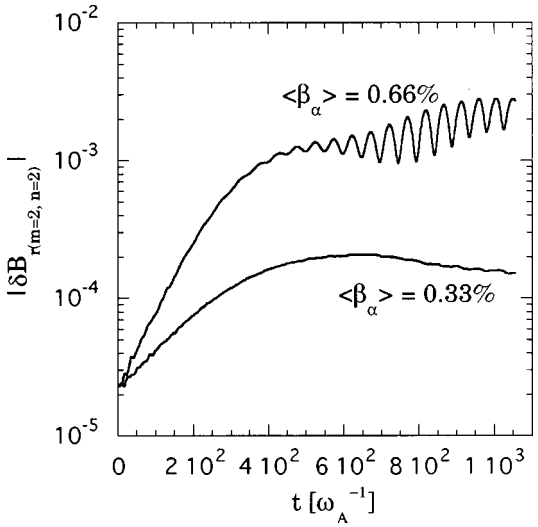

FIG. 3. Time evolution of the $m/n=2/2$ component of δB_r on $r=0.25a$ magnetic surface for (a) $\langle\beta_\alpha\rangle=0.33\%$, and (b) 0.66%.

$$l=-m \quad (V_m>0), \tag{33}$$

$$l=m \quad (V_m<0). \tag{34}$$

The dominant poloidal harmonics of the destabilized $n=2$ TAE mode are $m=2$ and $m=3$. Around $q=5/4$, V_m of $m=2$ and $m=3$ harmonics is positive and negative, respectively, since ω_0 is positive. Thus, far-passing particles with positive parallel velocities resonate with the $m=2$ harmonic with $l=-2$, while far particles with negative parallel velocities resonate with the $m=3$ harmonic with $l=3$.

We should notice that not only passing particles but also trapped particles are resonating with the TAE mode. This is an important point for the particle losses discussed in Sec. IV. The energy transfer from trapped particles accounts for 37% of the total energy transfer. We also show the l values of the top 8000 particles which cover 90% of the total energy transfer in Fig. 2(b). We can see that weakly resonant trapped particles fill the gaps among strongly resonant trapped particles in Fig. 2(a).

IV. NONLINEAR SIMULATION

Nonlinear simulations have been carried out for two initial alpha pressures, $\langle\beta_\alpha\rangle=0.33\%$ and 0.66%. For MHD equations, we use a finite difference method of fourth-order accuracy in space and time. The grid numbers used are (65,16,65) for (R,φ,z) coordinates, respectively, and 4×10^6 particles are used. The simulation domain in the toroidal direction is $0\leqslant\varphi\leqslant\pi$ since we focus on the $n=2$ TAE modes. The TAE mode which is found in the linear simulation is employed as the initial perturbation. Time evolutions of amplitude of the $m/n=2/2$ harmonic of δB_r at $r=0.25a$ magnetic surface are shown in Fig. 3. For $\langle\beta_\alpha\rangle=0.66\%$, the amplitude once reaches a plateau roughly between $t=400\omega_A^{-1}$ and $t=600\omega_A^{-1}$, and rises again accompanied by an oscillation. The instability saturates in $1000\omega_A^{-1}$ for both cases.

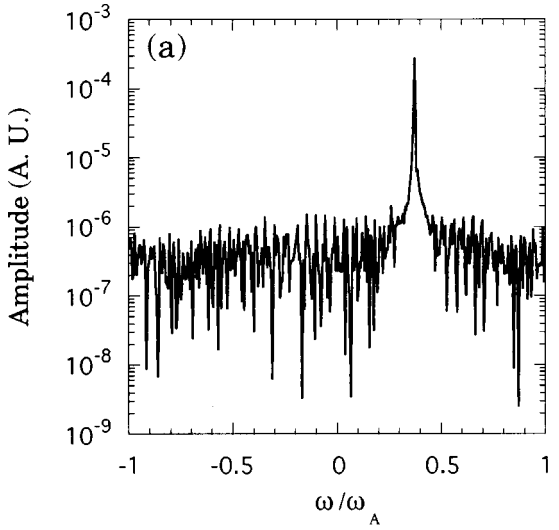

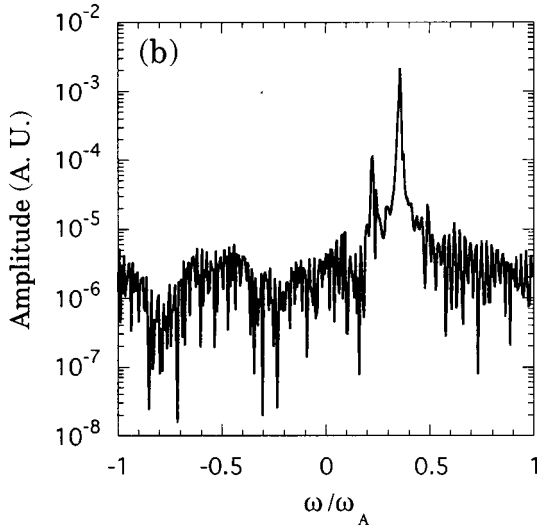

FIG. 4. Frequency spectrum of δB_r on $r=0.25a$ magnetic surface for (a) $\langle\beta_\alpha\rangle=0.33\%$, and (b) 0.66%. The peak of the second $n=2$ TAE mode appears at $\omega=0.22\omega_A$ in (b).

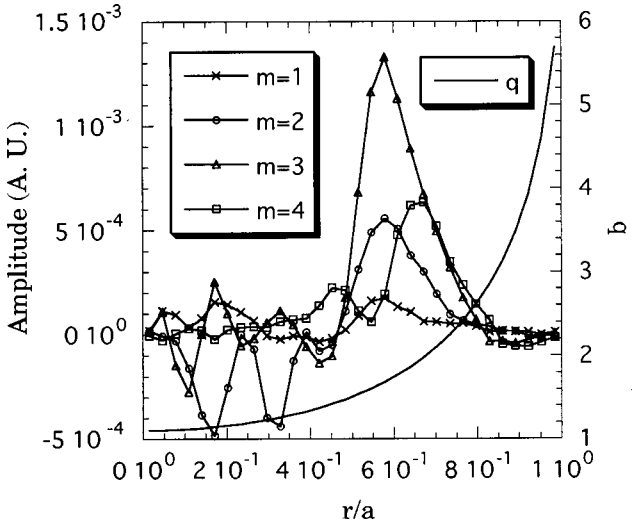

FIG. 5. Radial profiles of the dominant poloidal harmonics of the electrostatic potential for the second $n=2$ TAE mode.

Before turning to the saturation mechanism, we shall draw our attention to the oscillatory behavior of $\langle\beta_\alpha\rangle=0.66\%$. Frequencies of $m/n=2/2$ harmonic for two cases are analyzed and the results are shown in Fig. 4. In both cases one peak is seen around $\omega=0.36\omega_A$, which indicates that the TAE mode which is investigated with the linear simulation grows in both cases. In addition to it, a new mode is excited at $\omega=0.22\omega_A$ for $\langle\beta_\alpha\rangle=0.66\%$. This frequency suggests that the new mode is another $n=2$ TAE mode whose dominant poloidal harmonics are $m=3$ and $m=4$, since the frequency is close to, and lower by $0.06\omega_A$ than the gap center of $m/n=3/2$ and $m/n=4/2$ shear Alfvén continuum spectra at $q=7/4$. Poloidal harmonics of the new mode are obtained by subtracting those of the linear growth phase (at $t=198\omega_A^{-1}$) from those of the nonlinear phase (at $t=890\omega_A^{-1}$). The residual poloidal harmonics of the electrostatic potential are shown in Fig. 5. It is consistent with the theory of the TAE mode that the dominant harmonics are $m=3$ and $m=4$, which peak around the $q=7/4$ surface. Thus, we can conclude that the new mode is the second $n=2$ TAE mode whose major poloidal harmonics are $m=3$ and $m=4$. The oscillation of the amplitude in Fig. 3 is the beat between these two TAE modes. Hereafter, we refer to the $m/n=2,3/2$ TAE mode and the $m/n=3,4/2$ TAE mode as the ''first TAE mode'' and the ''second TAE mode,'' respectively.

We compare the electrostatic potential of a nonlinear phase with that of a linear phase. Figure 6 shows contours of the electrostatic potential on a poloidal plane of the linear phase (at $t=198\omega_A^{-1}$) and of nonlinear phases (at $t=865\omega_A^{-1}$ and at $t=890\omega_A^{-1}$). Compared with the linear phase, it can be seen that the second TAE mode broadens the distribution of the electrostatic potential outwards in the minor radius. At $t=865\omega_A^{-1}$ the two TAE modes are in phase, while they are out of phase at $t=890\omega_A^{-1}$. It is interesting to note that such coexistence of multiple TAE modes with the same toroidal mode number will be more likely for high toroidal mode numbers, since TAE modes locate spatially close to each other.

Let us turn our attention to the time evolution. Figure 7 shows time evolutions of the ratio of energy-transfer rate $\langle -\mathbf{j}_\alpha\cdot\mathbf{E}\rangle$ to the doubled energy of $n=2$ MHD modes for the two cases. For $\langle\beta_\alpha\rangle=0.33\%$, we can see that decrease in the energy transfer leads to saturation. This is consistent with the picture of the saturation due to the wave–particle trapping. On the other hand, for $\langle\beta_\alpha\rangle=0.66\%$ in Fig. 7(b), the behavior of the ratio is somewhat complicated as well as that of the amplitude in Fig. 3. It once approaches zero at $t=400\omega_A^{-1}$ and rises again with an oscillation. We can explain this behavior as follows. Two $n=2$ TAE modes are both linearly unstable, and the first TAE mode saturates at $t=400\omega_A^{-1}$. It is reflected in the plateau in amplitude and the first decrease in the energy transfer. The second TAE mode continues to grow after the saturation of the first TAE mode. Coexistence of two TAE modes gives rise to the oscillations in the amplitude and the ratio, and growth of the second TAE mode

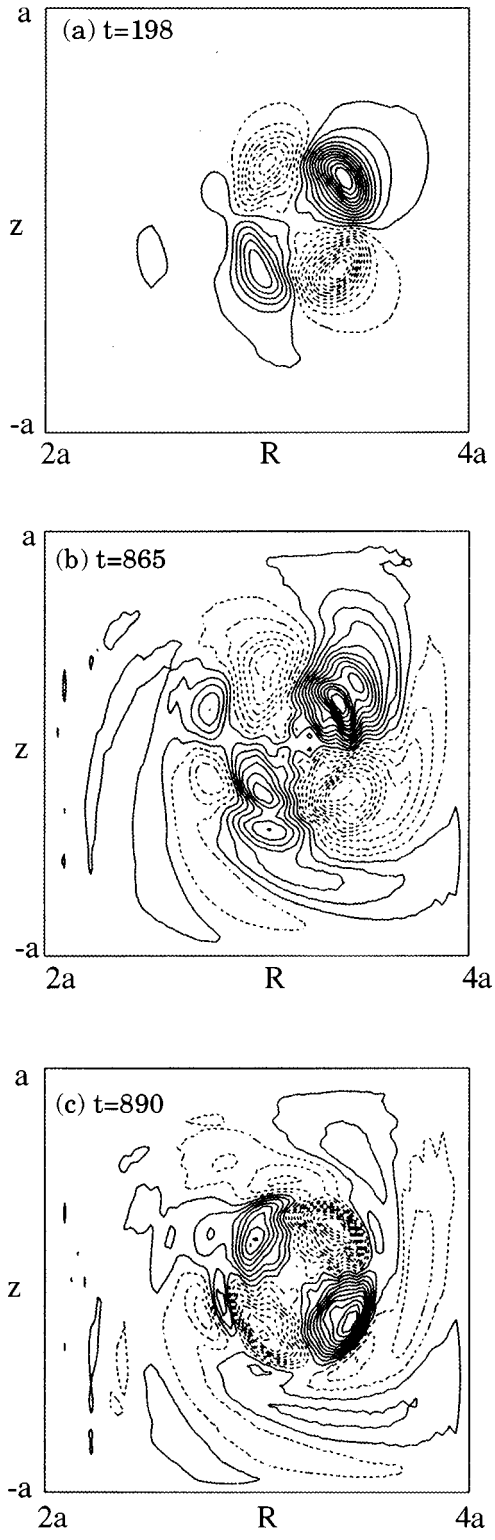

FIG. 6. Contours of the electrostatic potential on a poloidal plane for $\langle\beta_\alpha\rangle=0.66\%$ at (a) $t=198\omega_A^{-1}$, (b) $t=865\omega_A^{-1}$, and (c) $t=890\omega_A^{-1}$. Solid lines are for positive values and dashed lines are for negative values. Contour levels are normalized by temporal minimum and maximum values. Two TAE modes are in phase in (b), while they are out of phase in (c).

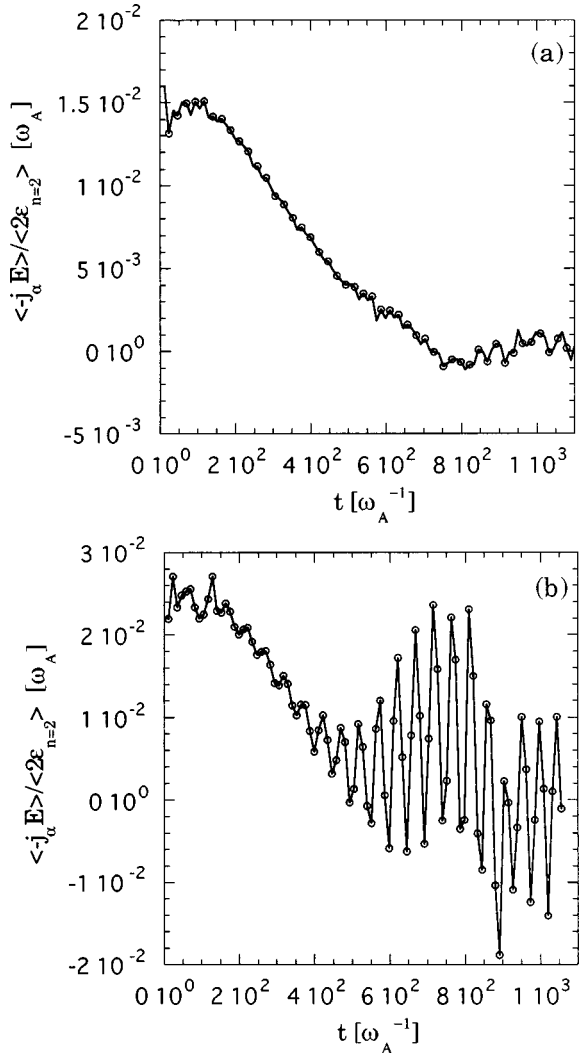

FIG. 7. Time evolution of the ratio of energy-transfer rate $\langle -\mathbf{j}_\alpha\cdot\mathbf{E}\rangle$ to doubled energy of $n=2$ MHD modes: (a) for $\langle\beta_\alpha\rangle=0.33\%$ and (b) for $\langle\beta_\alpha\rangle=0.66\%$. Decrease in the energy transfer leads to saturation of TAE instability in both cases.

increases the total amplitude. The rise in the ratio after $t=600\omega_A^{-1}$ is caused by the increase in the relative amplitude of the second TAE mode. Finally, saturation of the second TAE mode leads to the entire saturation. It is similar to the $\langle\beta_\alpha\rangle=0.33\%$ case that the decrease in the energy transfer leads to saturation, and it is also consistent with the picture of saturation due to wave–particle trapping. We cannot say for certain whether the resonance overlap has not happened between the two $n=2$ TAE modes, since we cannot investigate independent behaviors of two TAE modes.

TAE modes induced alpha-particle losses in the nonlinear simulations. The number ratio of lost particles to total alpha particles for $\langle\beta_\alpha\rangle=0.33\%$ and 0.66% are 1.4×10^{-5} and 1.2×10^{-2}, respectively. They differ from each other by three orders of magnitude. The saturation levels are 2×10^{-4} and 2×10^{-3}, respectively (see Fig. 2), and they differ by only one order of magnitude. It is consistent with the results of Ref. 2 that $\delta B\sim10^{-3}$ is the threshold for significant alpha-particle losses.

The distribution of TAE-induced lost-particles for $\langle\beta_\alpha\rangle=0.66\%$ in the initial minor radius and pitch angle is shown in Fig. 8. Lost particles can be classified into three types; (1) passing particles with negative parallel velocities (counter-passing particles) which cross the passing-trapped boundary

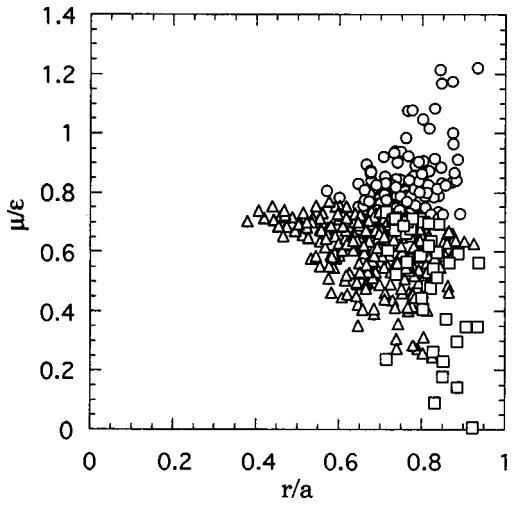

FIG. 8. Initial distribution of lost alpha particles in the $(r, \mu/\epsilon)$ plane, where μ and ϵ are magnetic moment and energy. Triangles denote counterpassing particles which finally become trapped particles. Interaction with the TAE modes changes them into trapped particles whose orbits connect with the wall. Circles and squares denote trapped particles and the other passing particles, respectively.

just before encountering the wall, (2) trapped particles, (3) passing particles other than the first type. Percentages to the total number of lost particles are 63%, 26%, and 11%, respectively. It is clear that counterpassing particles are the major part of lost particles and the main loss mechanism is crossing the passing-trapped boundary in the phase space. It is consistent with the results of test particle simulation in Ref. 2. It must be noted, however, that the trapped particles near this boundary are also lost in addition to the counterpassing particles. This is a reasonable result since we have found in the linear simulation that trapped particles also resonate with the TAE mode.

V. SUMMARY

We have developed new linear and nonlinear particle-MHD simulation codes and demonstrated that they are useful tools for studying linear and nonlinear TAE dynamics such as the mode structure, resonance condition, and alpha-particle losses. The resonance condition of alpha particles with the TAE mode is studied with a linear simulation. The resonance condition $\omega_0 - n\omega_\varphi - l\omega_\theta = 0$ (l: integer) is satisfied for strongly resonant particles. Weakly resonant particles fill gaps between strongly resonant particles in the $\omega_\varphi - l$ plane. Not only passing particles but also trapped particles resonate with the TAE mode.

Two nonlinear simulations are carried out for $\langle \beta_\alpha \rangle$ of 0.33% and 0.66%. An $n=2$ TAE mode whose dominant poloidal harmonics are $m=2$ and $m=3$ (the first TAE mode) is destabilized in both cases. For $\langle \beta_\alpha \rangle = 0.66\%$, another $n=2$ TAE mode whose dominant poloidal harmonics are $m=3$ and $m=4$ is destabilized in addition to the first TAE mode. Such coexistence of multiple TAE modes with the same toroidal mode number will be more likely for higher toroidal mode numbers, since each TAE mode is located spatially closer to one another.

Alpha particles are lost by TAE modes in the nonlinear simulation. Distribution of the lost particles in the initial phase space is analyzed. Counterpassing particles are the major part of lost particles. Interaction with the TAE modes changes them into trapped particles whose orbits connect with the wall. In addition to the counterpassing particles, trapped particles are also lost. This is reasonable since we have found in the linear simulation that trapped particles also resonate with the TAE mode.

Resonance overlap is predicted to take place when multiple TAE modes are destabilized.[9] In such cases, the wave–particle trapping will be prevented by the other TAE modes from working as a dominant saturation mechanism. This strongly indicates to us that the saturation level and saturation mechanism should be studied with nonlinear MHD equations. The nonlinear particle–MHD simulation code presented in this paper is a useful tool for future studies of the nonlinear evolution of multiple n TAE modes.

ACKNOWLEDGMENTS

The authors would like to express their thanks to all members of the Complexity Simulation Group for useful discussions. One of the authors (Y.T.) sincerely thanks Dr. J. W. Van Dam, Dr. H. L. Berk, Dr. B. N. Breizman, and other members of Institute for Fusion Studies, University of Texas at Austin for their kind hospitality and valuable discussions during his stay under the US–Japan JIFT exchange program. Numerical computations were performed at the Advanced Computing System for Complexity Simulation of National Institute for Fusion Science.

This work was partially supported by Grants-in-Aid of the Ministry of Education, Science and Culture (Nos. 07832024, 07858057, and 09878090).

[1] C. Z. Cheng and M. S. Chance, Phys. Fluids **29**, 3659 (1986).
[2] D. J. Sigmar, C. T. Hsu, R. White, and C. Z. Cheng, Phys. Fluids B **4**, 1506 (1992).
[3] B. N. Breizman, H. L. Berk, and H. Ye, Phys. Fluids B **5**, 3217 (1993).
[4] G. Y. Fu and W. Park, Phys. Rev. Lett. **74**, 1594 (1995).
[5] Y. Todo, T. Sato, K. Watanabe, T. H. Watanabe, and R. Horiuchi, Phys. Plasmas **2**, 2711 (1995).
[6] Y. Wu, R. B. White, Y. Chen, and M. N. Rosenbluth, Phys. Plasmas **2**, 4555 (1995).
[7] C. Z. Cheng, R. V. Budny, L. Chen, M. S. Chu, D. S. Darrow, E. D. Fredrickson, G. Y. Fu, T. S. Hahm, C. T. Hsu, E. Mazzucato, H. E. Mynick, R. Nazikian, W. Park, N. Pomphrey, D. J. Sigmar, R. B. White, Y. Wu, and S. J. Zweben, in *Plasma Physics and Controlled Nuclear Fusion Research 1994* (International Atomic Energy Agency, Vienna, 1996), Vol. III, p. 373.
[8] J. Candy and M. N. Rosenbluth, Nucl. Fusion **35**, 1069 (1995).
[9] H. L. Berk, B. N. Breizman, and M. Pekker, Phys. Plasmas **2**, 3007 (1995).
[10] D. A. Spong, B. A. Carreras, and C. L. Hedrick, Phys. Plasmas **1**, 1503 (1994).
[11] F. Zonca, F. Romanelli, G. Vlad, and C. Kar, Phys. Rev. Lett. **74**, 698 (1995).
[12] W. Park, S. Parker, H. Biglari, M. Chance, L. Chen, C. Z. Cheng, T. S. Hahm, W. W. Lee, R. Kulsrud, D. Monticello, L. Sugiyama, and R. White, Phys. Fluids B **4**, 2033 (1992).
[13] A. M. Dimits and W. W. Lee, J. Comput. Phys. **107**, 309 (1993).
[14] S. E. Parker and W. W. Lee, Phys. Fluids B **5**, 77 (1993).
[15] Y. Todo and T. Sato, ''A Particle Algorithm for Linear Kinetic Analysis in Tokamak Plasmas,'' to appear in J. Comput. Phys.